

AERODYNAMIC DESIGN OPTIMIZATION OF A NON-PLANAR C-WING CONFIGURATION

Hulya Sukas¹, Berkay Pirlepel², Kiran Ramesh³, Melike Nikbay⁴, Konstantinos Kontis⁵
Istanbul Technical University; University of Glasgow
Istanbul, TURKEY; Glasgow, SCOTLAND

ABSTRACT

The main goal of aircraft preliminary design is to enhance the aerodynamic performance of wings, and hence an optimization procedure is essential. In this study, the aerodynamic performance of non-planar wings is numerically investigated under different incidences and validated against experiments [8]. Subsequently, a design optimization study of a non-planar “C-wing system is carried out by considering certain constraints and design parameters. Three variables are selected as optimization variables and a sampling study is performed using the LHS method with random selections. A surrogate model is created using the sampling results and the optimization process is carried out using this model.

Keywords: C-wing; optimization; induced drag; RANS; non-planar wing

INTRODUCTION

Researchers around the world have made various design optimizations to reduce the fuel consumption of air vehicles. It has been shown that non-planar wing systems have some benefits on aerodynamic performance compared to traditional wings. For this reason, many new configurations have been developed so far. To improve the aerodynamic performance, an implementation of a framework which includes numerical methods and optimization drivers must be considered.

In this study, the design optimization of a non-planar wing has been performed to increase its aerodynamic efficiency. In this context, the aerodynamic characteristics of the C-wing configuration were investigated. In the first phase of the study, validation of the numerical model was done for a various angle of attacks using the data of [Skinner, 2018]. In the second step, aerodynamic optimization of the initial C-wing geometry was carried out using the three selected design variables of the geometry. To perform this optimization process, an algorithm which

1 Master student, Istanbul Technical University, Email: hulyaistifsukas@gmail.com

2 Master student, Istanbul Technical University, Email: berkay270@gmail.com

3 Lecturer, University of Glasgow, Email: kiran.ramesh@glasgow.ac.uk

4 Professor, Istanbul Technical University, Email: nikbay@itu.edu.tr

5 Professor, in University of Glasgow, Email: kostas.kontis@glasgow.ac.uk

connects the pre-processing tool and flow solver was used, and these calculations were done automatically within the optimization framework. Therefore, all aerodynamic analyses and design optimization processes were run together in a loop utilizing the codes developed.

NUMERICAL SETUP

In this section, we describe the numerical setup which is validated against experimental data for both planar and C-wing configurations published in [Skinner, 2018]. Experimental conditions were reproduced exactly the same using Computational Fluid Dynamics (CFD) approach.

Figure 1 shows the geometrical information of wings. C-wing configuration is composed of three parts which are top-wing, side-wing and main wing. The wing tip is bent like the letter “C” to reduce the tip vortices.



Figure 1: Planar and non-planar wing systems.

Since there is a symmetrical flow around aircraft, only half body was modelled in numerical simulations as shown in Figure 2.

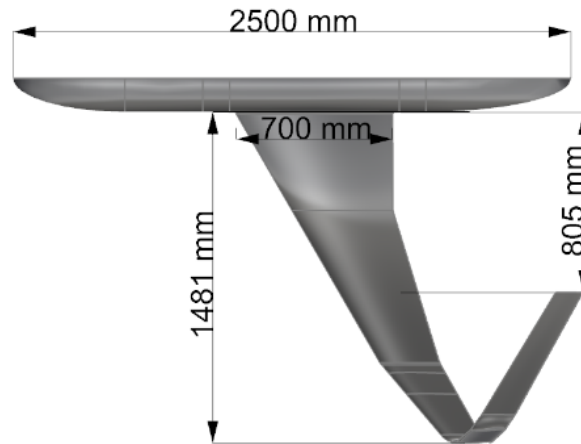


Figure 2: Main dimensions of half body of aircraft.

Control volume and boundary conditions must be defined for the numerical solution as an Eulerian approach is used. The diameter of control volume (computational domain) was selected four times the length of the fuselage as shown in Figure 3. Boundary conditions implemented for the control volume are given as velocity inlet for far-field, slip wall for symmetry plane and no-slip wall for the body.

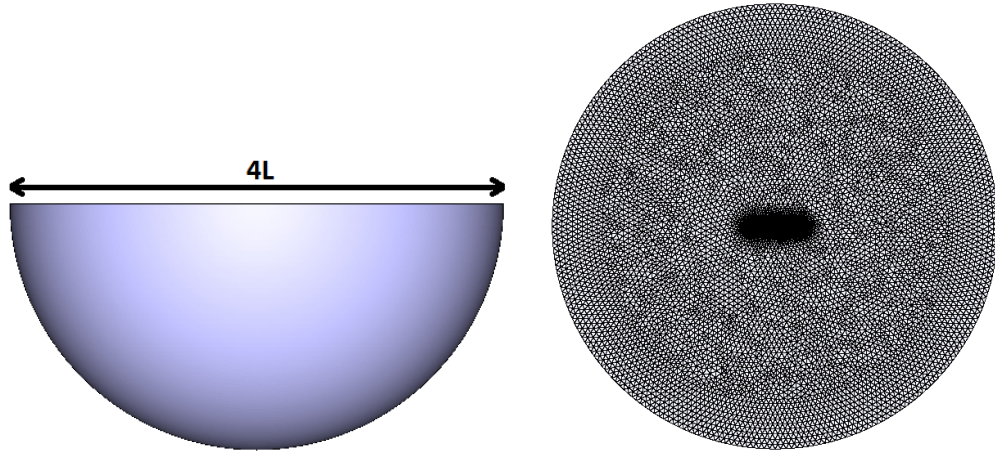


Figure 3: Semi spherical flow domain (left), and a sectional view of the symmetry plane (right).

In this study, Pointwise software was used for the generation of both surface and volume meshes. The mesh quality has been improved in sensitive areas such as the boundary layer, wingtip and wing vicinity to capture flow fields accurately. In Figure 4, the growth of grid elements can be seen around the whole geometry and it is obvious that grid size is coarser in the far-field. Since capturing flow separations are quite important to get accurate results around the wing, mesh resolution near the leading and trailing edges of the wing must be higher. Therefore, quad elements were generated in these regions.

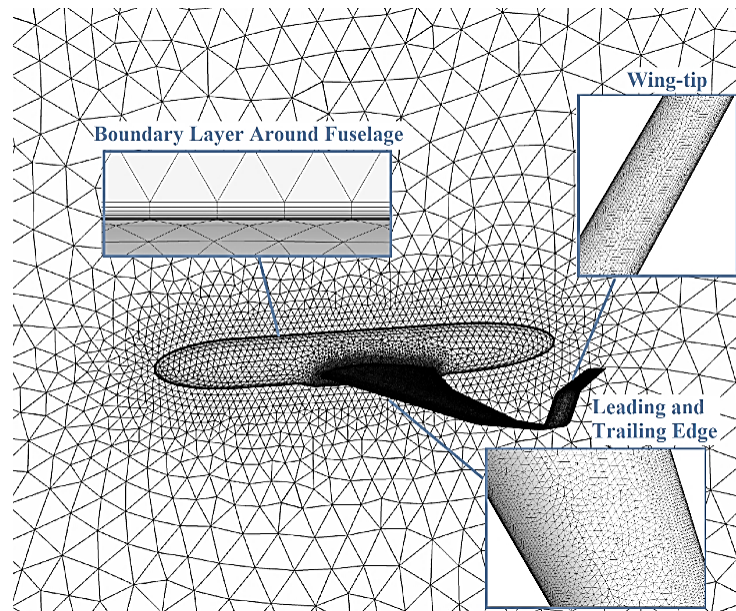


Figure 4: Distribution of surface and volume meshes in the computational domain.

The total thickness of the boundary layer is calculated using Prandtl's boundary layer formula for turbulent flows, which is given in equation 1. Boundary-layer mesh generated around the wing can be seen in Figure 5.

$$\delta_{BL} = \frac{0.16 x}{\Re_x^{\frac{1}{7}}} \quad (1)$$

The growth rate between prism layers and the total number of layers were determined according to first layer thickness and the total thickness of the boundary layer. Detailed information about the boundary layer thickness is given in Table 1. The cell count of various element types in the mesh are given in Table 2.

Table 1: Boundary layer parameters for wing and fuselage.

First Layer Thickness	0.007
Growth Rate	1.4
Number of Layers	19

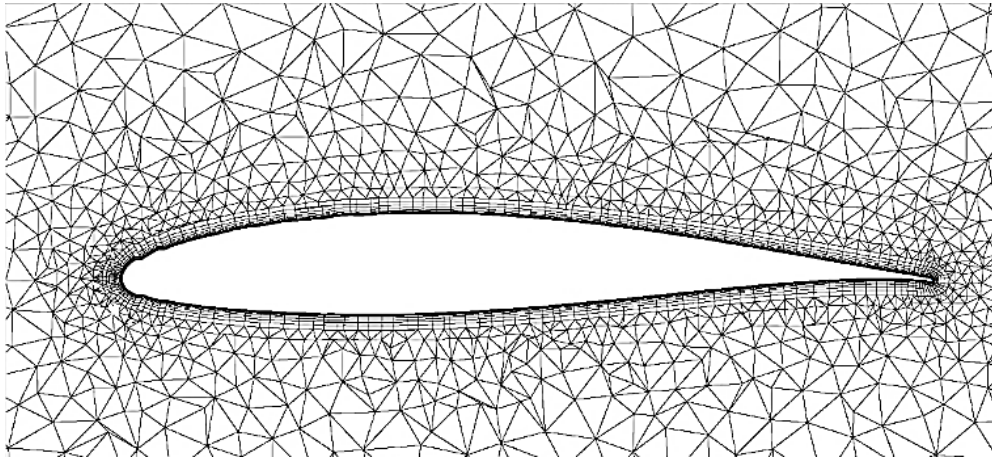


Figure 5: Boundary layer development around the wing.

After grid generation is completed, a physical model for flow solver was set up. For numerical simulations, a RANS based CFD solver Star-CCM+ was used. The setup parameters of the physical model can be seen in Table 3. The experimental conditions used for the numerical simulations are given in Table 4.

Table 2: Flow properties in the RANS simulations performed.

Surface Mesh		Volume Mesh			Total Domain
Quad	Triangles	Tetrahedral	Pyramids	Prisms	Total Cell
2318	124600	2522986	2608	1599076	4124670

Table 3: Physical model parameters used in Star-CCM+.

Flow property	Implicit Unsteady
Material property	Constant Air
Flow model	Segregated Flow
Viscous regime	Turbulent Flow
Turbulence model	$SST k-\omega$
Time step size	0.02

Table 4: Flow properties in the RANS simulations performed.

Parameters	Units	Value
Mach Number	-	0.41
Altitude	m	0
Dynamic Pressure	Pa	1532.25
Angle of Attack	deg	0,2,4,6,8,10,12

The RANS (Reynolds Averaged Navier-Stokes) equations were solved to calculate the velocity and pressure distribution in the computational domain. Since the current Mach number is sufficiently low (<0.30), the effect of compressibility was neglected in the simulations. All y^+ value was set to be lower than one and $SST k-\omega$ turbulence model was used to include turbulence effects into the solutions.

OPTIMIZATION FRAMEWORK

To establish an optimization framework, it is necessary to select proper optimization variables and criteria applicable to a parametric model. In this study, Latin Hypercube sampling method was used to choose optimization parameters. In short, this method creates optimization cases after shuffling the selected parameters randomly.

It is also desired to see the results at intermediate points in between the samples considered. Since performing CFD analyses for every single point is computationally expensive, a surrogate model was created by using the results obtained in sampling simulations. Kriging method is used to generate the surrogate model.

As mentioned above, the analyses and optimization tools used here are coupled with each other as shown in Figure 6. Initially, a representative parametric model is created in the loop, then this model is exported to the grid generation tool to discretize the body and computational domain. Subsequently, this discretized domain is sent to flow solver and simulation is performed until convergence is achieved.

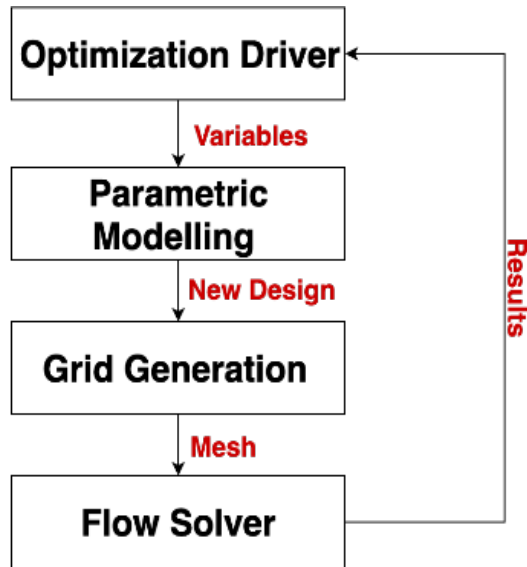


Figure 6: Workflow diagram of the CFD based optimization study.

RESULTS

Validation of the numerical model

StarCCM+ was used as an incompressible RANS based solver for numerical simulations, and numerical results obtained were compared with experimental data [8] in terms of drag and lift coefficients. A flow simulation converges in approximately 40 minutes using the current numerical model. Figure 7 shows the comparison of numerical results with experimental data for the planar wing and C-wing configurations for various incidences.

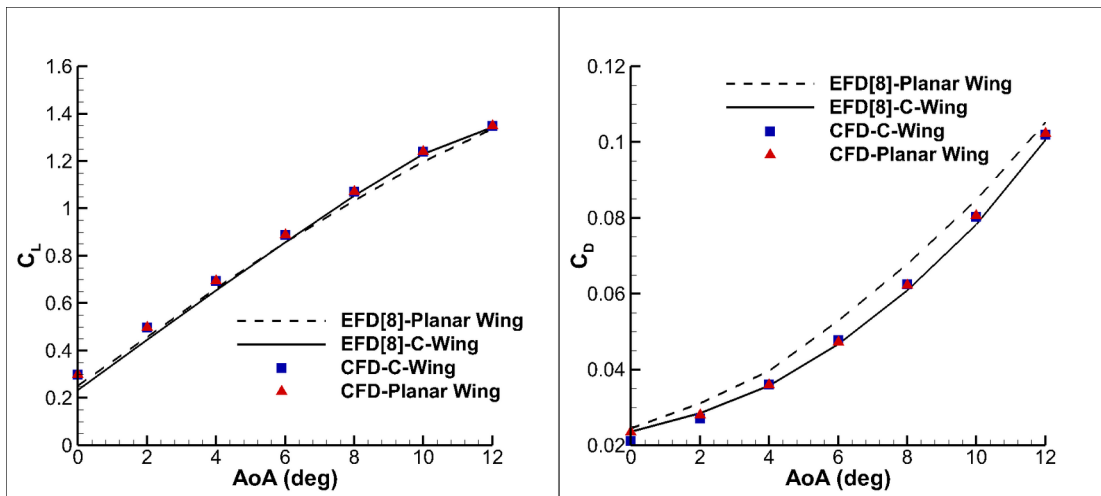


Figure 7: Lift (left) and drag (right) coefficients for different AoAs.

According to experimental data, it can be seen that the planar wing produces more drag force than C-wing configuration. This phenomenon can be explained by the reduction of tip vortices (induced drag) in the C-wing design. In Figure 7, numerical results of C_D and C_L seem to be compatible with experimental data even for higher AoAs ($>10^\circ$). Average relative errors for C_D

and C_L were calculated at reasonable levels of accuracy such as 8% and 6% for the planar wing, while they are 1.5% and 3.0% for C-wing. Figure 8 shows the comparison of aerodynamic efficiency (C_L/C_D) of C-wing configuration.

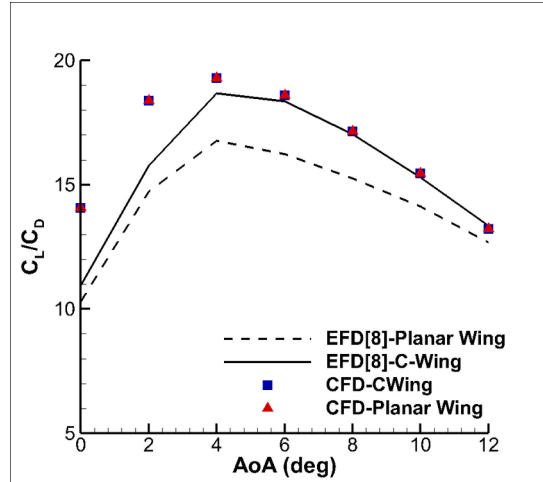


Figure 8: Comparison of experimental and numerical results for planar and C-wing configurations in terms of aerodynamic efficiency (C_L/C_D).

According to Figure 8, numerical results agree well with the experiments with an average relative error of 2.4%. It can also be noted that the difference between the two configurations becomes clear between $2^\circ < \text{AoA} < 8^\circ$. This indicates the high aerodynamic efficiency of C-wing compared to traditional wing designs due to reduction of tip vortices at the tip of the wings.

As widely known, induced drag is the drag component caused by the production of lift by the lifting surfaces, which can include the fuselage as well as the wings and tail. Parasitic drag is composed of form drag, skin friction drag, and interference drag. In this context, total drag force coefficient predicted in numerical simulations was divided into shear (parasitic drag) and pressure (induced drag) components and it was deduced that a considerable portion of the total drag force is composed of induced drag. Figure 9 shows the induced drag and total drag coefficients. Approximately, the induced drag component constitutes 40% of the total drag force for $\text{AoA}=0$. However, this ratio tends to increase up to 85% at $\text{AoA}=12$. It should be noted that these proportions of induced drag were obtained at one speed ($M=0.41$), it may decrease as the speed of aircraft increases.

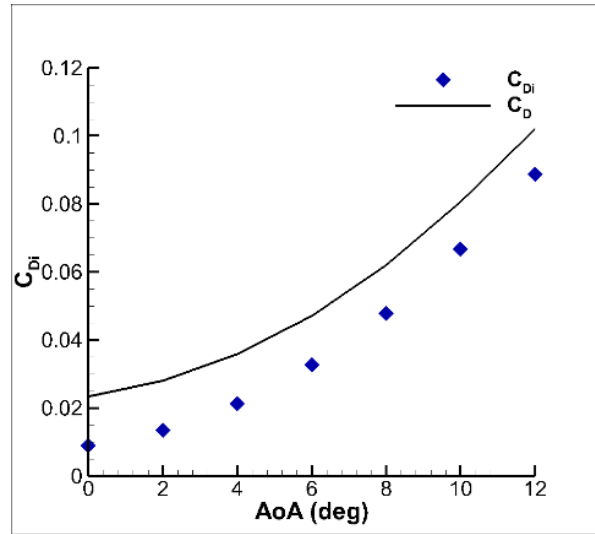


Figure 9: Total drag and induced drag coefficients of C-wing configuration for various AoAs.

Optimization Methodology and Results

In this study, an optimization study was carried out to obtain the optimum wing geometry which gives maximum aerodynamic efficiency (C_L/C_D). In Figure 10, three selected optimization variables are shown. The methodology used for the optimization process is as follows:

- A certain number of high-fidelity simulations must be performed to create a surrogate model. Therefore, optimization variables (a , b , ϕ) randomly selected by LHS (Latin Hypercube Sampling) method in Dakota.
- Values of optimization variables which are transferred from Dakota are updated in the parametric model.
- The computational mesh is generated by AM (Aircraft Mesher) using the parametric model and it is exported to incompressible RANS solver (Star CCM+) to obtain numerical results (C_L, C_D).
- Finally, using the Conjugate Gradient and Quasi-Newton methods with two different Hessian approaches, optimum geometries are obtained in terms of aerodynamic efficiency (C_L/C_D).

Using the LHS method, these variables were shuffled, and random scenarios were created. In this study, a total of 25 samples were generated according to the variables shown in Figure 10.

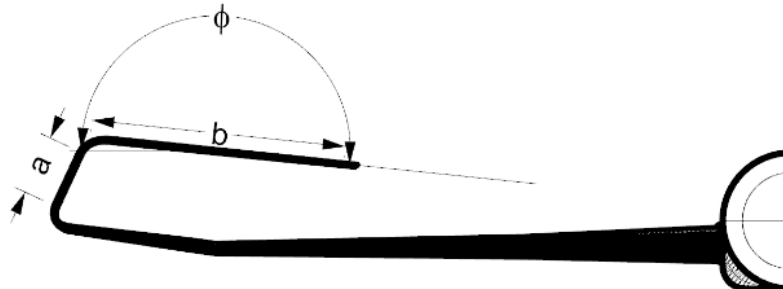


Figure 10: Optimization variables for C-wing geometry.

The optimization problem in this study can be defined as:

$$\max \left(\frac{C_L}{C_D} \right)$$

$$\text{subject to : } g_1(s) = 0.4 < a + b < 0.6$$

$$g_2(s) = C_L > C_{L\text{original}}$$

$$\vec{s} = \{a, b, \phi\}$$

$$s_l = \{0.01, 0.40, 90\}$$

$$s_u = \{0.15, 0.70, 220\}$$

For the samples of interest, all flow analyses were run and each of the results obtained was saved in a separate working directory. Considering that each analysis takes an average of 40 minutes, the total calculation time to complete the optimization process is approximately 17-18 hours.

Table 5: Optimization variables under certain constraints.

	$a(m)$	$b(m)$	$\phi(deg)$
Lower Bound	0.0100	0.4000	90.00
Upper Bound	0.1500	0.7000	220.00
Original Values	0.1250	0.5510	186.10
Optimum Values (CGM)	0.0365	0.5634	172.42
Optimum Values (QNM-FDM)	0.0240	0.5759	177.09
Optimum Values (QNM-BFGS)	0.0127	0.5872	182.20

To examine the accuracy of the surrogate model, three random cases were created. The flow analyses were performed in STAR CCM+ and the results were compared against those of the surrogate model. All results are given in Table 6.

Table 6: Comparison of results obtained by flow solver and surrogate model.

		Case I	Case II	Case III
Parameters {a, b, ϕ }		{0.09 0.45 120}	{0.12 0.65 190}	{0.14 0.56 210}
High-Fidelity Flow Solver	C_L	0.1884	0.1642	0.1750
	C_D	0.0232	0.0242	0.0241
	$\frac{C_L}{C_D}$	8.1215	6.7867	7.2252
Surrogate Model	C_L	0.1794	0.1659	0.1788
	C_D	0.0187	0.0219	0.0220
	$\frac{C_L}{C_D}$	9.5935	7.5753	8.1272

For C_L , the relative error of the surrogate model was found between 2-4%, while it was calculated as 10% for C_D . High-fidelity analysis takes approximately 40 minutes but the surrogate model gives results in less than one minute.

Weight of the wing can also be restricted by limiting the value of $a+b$ which governs the C-wing tip height and length. Considering the constraints given, the objective function was maximized using three different optimization methods in Dakota. According to Table 6, it can be stated that aerodynamic efficiency increases with the increment in dihedral angle, and decreases with values of a and b. The values obtained for original and optimum geometries are compared in Table 7.

Table 7: Aerodynamic forces for optimum and original geometry.

	Original Geometry	Optimum Geometry (CGM)	Optimum Geometry (QNM-FDM)	Optimum Geometry (QNM-BFGS)
C_L	0.1705	0.1708	0.1707	0.1706
C_D	0.0220	0.0216	0.0215	0.0217
$\frac{C_L}{C_D}$	7.7500	7.9071	7.9395	7.8617

Geometrical representations of three different methods can also be examined in Figure 11. The geometries coloured by grey indicate the original design, while optimum designs show the optimized geometries. Figure 12 shows the change in objective function depending on the iteration number. Since a gradient-based algorithm which generally provides a quick convergence speed was used, the cost function converged in eight iterations under given constraints. In this study, the tolerance for relative error between two iterations was given as 10^{-5} . When relative error reaches this value, Dakota kills the optimization process automatically.

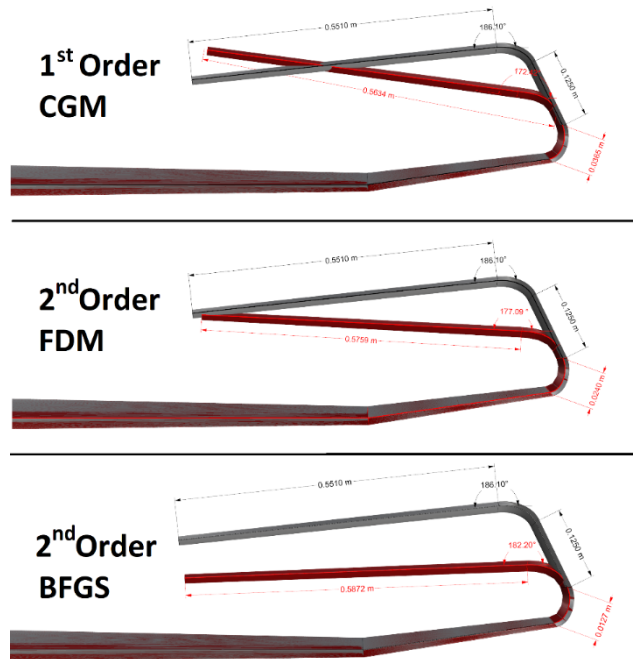


Figure 11: Comparison of the original geometry (grey) and optimum geometry (red) in terms of aerodynamic efficiency (C_L/C_D) for three different optimization methods.

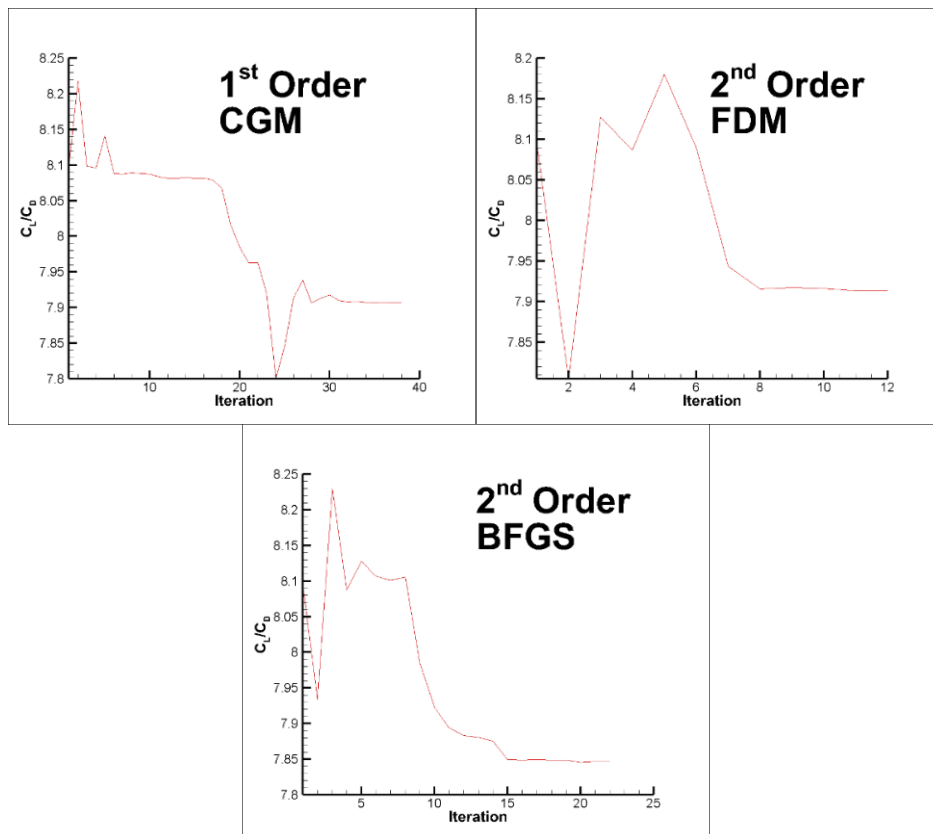


Figure 12: Optimization history for each method according to iteration and cost function for 10^{-5} convergence tolerance.

Function evaluation and iteration number of the three optimization methods can be found in Table 8. It can be said that even though Quasi-Newton with FDM did highest function evaluation in three of them, it has the fastest convergence among all.

Table 8: Number of function evaluation and iteration number of optimization methods.

	Number of Function Evaluation	Iteration Number
CGM	98	38
QN (BFGS)	154	22
QN (FDM)	516	12

It is also possible to examine pressure distribution on the aircraft for both original and optimum geometries in Figure 13. Since all optimum geometries have similar pressure distribution, only one of them was used to make a comparison. According to Table 8, Quasi-Newton which uses the Finite Difference Method to determine the Hessian matrix gives the best aerodynamic efficiency.

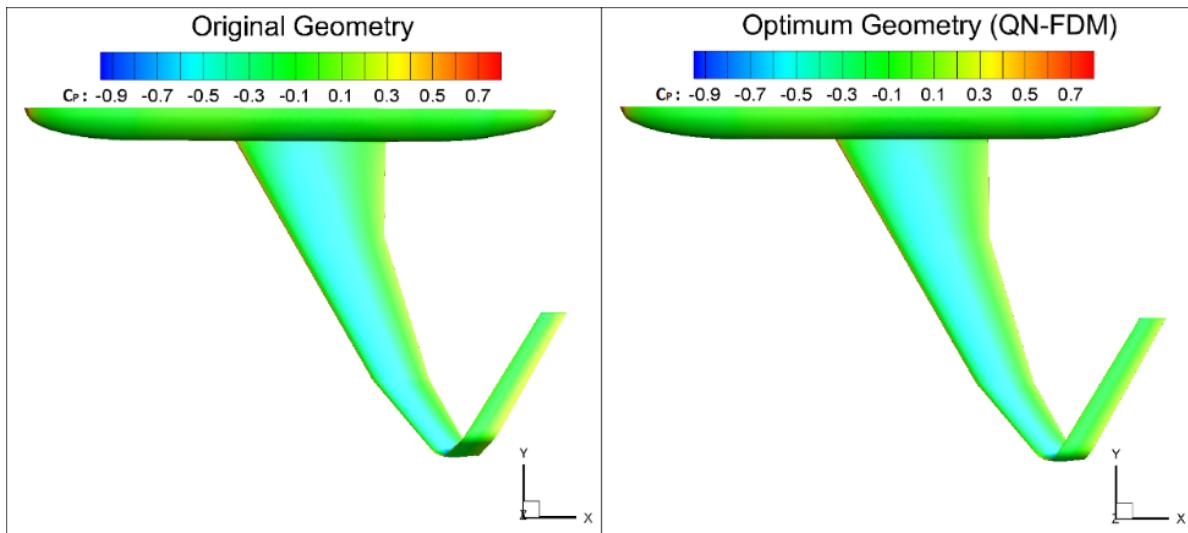


Figure 13: Pressure distribution for original geometry and optimum geometry by QN-FDM.

It can be seen from Figure 13 that the pressure distribution on the tip of the original wing is higher than that of the optimum design. This shows that less lift force occurs on the original geometry compared to optimized wing design.

The design purpose of the C-wing configuration is to produce lower induced drag compared to the planar wing. After optimum geometry was obtained in terms of aerodynamic efficiency, streamlines for optimum and original geometry are shown in Figure 14. Since aerodynamic efficiency was found higher than the other optimization method using QN-FDM approach, only this geometry was compared with the initial C-wing geometry showing the streamlines. It can be seen that the velocity gradient of the original C-wing geometry is greater than the optimum one, especially on the wingtip. Therefore, there will be a higher induced drag on the original geometry.

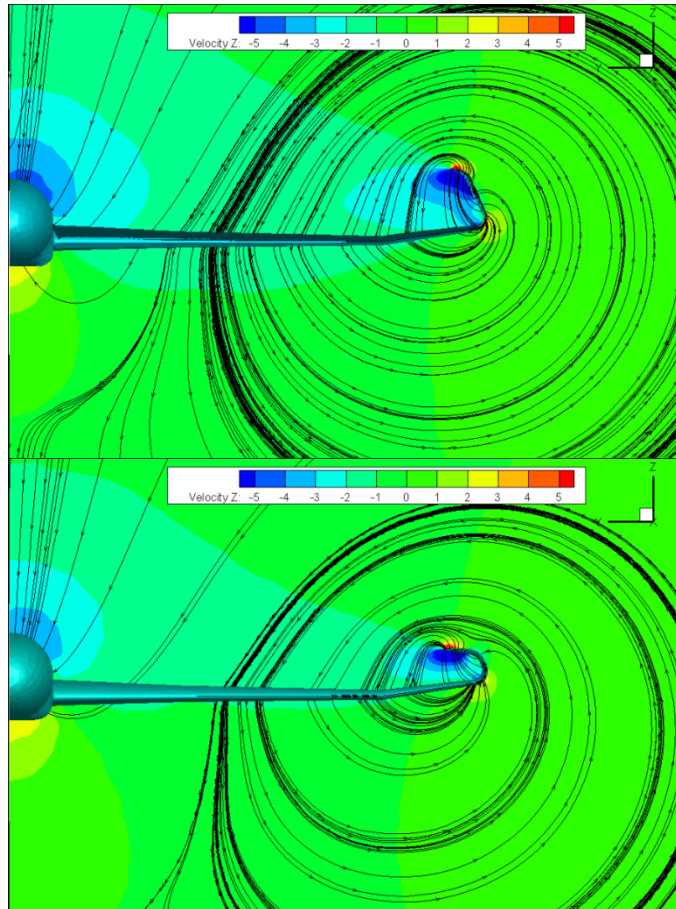


Figure 14: Streamtraces for the initial (top) and optimum (bottom) C-wing geometry (QN-FDM) at zero angle of attack.

CONCLUSIONS

In this study, flow around C-wing configuration was numerically investigated and the original geometry was optimized to increase aerodynamic efficiency. It was aimed to increase efficiency as much as possible under certain constraints. In the first part of the study, validation of the numerical model was carried out using experimental data [8]. It was shown that our numerical model is accurate enough so that the numerical results agree well with experimental data. Secondly, optimum geometry for C-wing was investigated to increase aerodynamic efficiency. In this context, an optimization framework was established and multiple tools were integrated. Several scripts were developed for these tools to work together. After the CFD-based optimization framework has been created, the optimization problem was defined successfully. Three variables were selected as optimization variables and a sampling study was performed using the LHS method with random selections. A surrogate model was created using the sampling results and the optimization process was carried out using these models. The aerodynamic efficiency of optimized geometry was found higher than the original one as we expected, and therefore the goal of this study was accomplished.

In future work, it is planned to perform an optimization study for the same geometry including the effects of aero-structural interactions into the problem.

Acknowledgements

The authors would like to thank Dr Shaun N. Skinner and Dr Hossein Zare-Behtash for providing the geometry and experimental data [Skinner, 2018] for the numerical validation study in this paper.

References

- [1] **Adams et al. (2018)**. "Dakota, A Multilevel Parallel Object-Oriented Framework for Design Optimization, Parameter Estimation, Uncertainty Quantification, and Sensitivity Analysis: Version 6.9 User's Manual"
- [2] **Armstrong, M., (1998)**. "Basic Linear Geostatics" Springer-Verlag Berlin Heidelberg, Newyork.
- [3] **Arora, J.S., (2016)**. "Introduction to Optimum Design", Elsevier, England.
- [4] **CD-Adapco, (2017)**. User Guide STAR-CCM+ Version 12.02.
- [5] **Fletcher, C.A.J., (1991)**. "Computational Techniques for Fluid dynamics I -Fundamental and General Techniques", Springer-Verlag, Newyork.
- [6] **NASA (2014)**. User Manual OpenVSP V3.17.0.
- [7] **Schneider, W., (2001)**. "The importance of aerodynamics in the development of commercial successful transport aircraft," Page 9-16, Notes on Numerical Fluid Mechanics. Bremen, Springer.
- [8] **Skinner, S.N, (2018)**, "Study of a C-wing Configuration for Passive Drag and Load Alleviation", PhD Thesis, University of Glasgow, June
- [9] **Pointwise (2016)**. User Guide V18.0R1.
- [10] **Travis Carrigan Aircraft Mesher Script for Pointwise Retrieved: 01/03/2019** from <https://github.com/pointwise/AircraftMesher/blob/master/AircraftMesher.glf>
- [11] **Versteeg, H.K., Malalasekera, W. (2007)**. "An Introduction to Computational Fluid Dynamics", Pearson Education, England.
- [12] **White, F.M & Corfield, I. (2006)**. "Viscous fluid flow" (Vol. 3, pp. 433-434). New York: McGraw-Hill.